# Supplementary Information: Spin signatures in the electrical response of graphene nanogaps

Víctor M. García-Suárez,[a,b] Amador García-Fuente,[a] Diego J. Carrascal,[a,b] Enrique Burzurí,[*,c,d] Max Koole,[c] Herre S. J. van der Zant,[c] Maria El Abbassi,[e,f] Michel Calame,[e,f] and Jaime Ferrer[*,a,b]

[a] *Departamento de Física, Universidad de Oviedo, 33007 Oviedo, Spain.*

[b] *Nanomaterials and Nanotechnology Research Center CINN, CSIC-Universidad de Oviedo, El Entrego, Spain.*

[c] *Kavli Institute of Nanoscience, Delft University of Technology, PO Box 5046, 2600 GA Delft, The Netherlands.*

[d] *IMDEA Nanoscience, Ciudad Universitaria de Cantoblanco, C/Faraday 9, 28049 Madrid, Spain. E-mail: enrique.burzuri@imdea.org*

[e] *Department of Physics, University of Basel, Klingelbergstrasse 82, CH-4056, Basel, Switzerland.*

[f] *Empa, Swiss Federal Laboratories for Materials Science and Technology, Uberlandstrasse 129, CH-8600 Dubendorf, Switzerland.*

# 1 Fabrication and experimental measurements

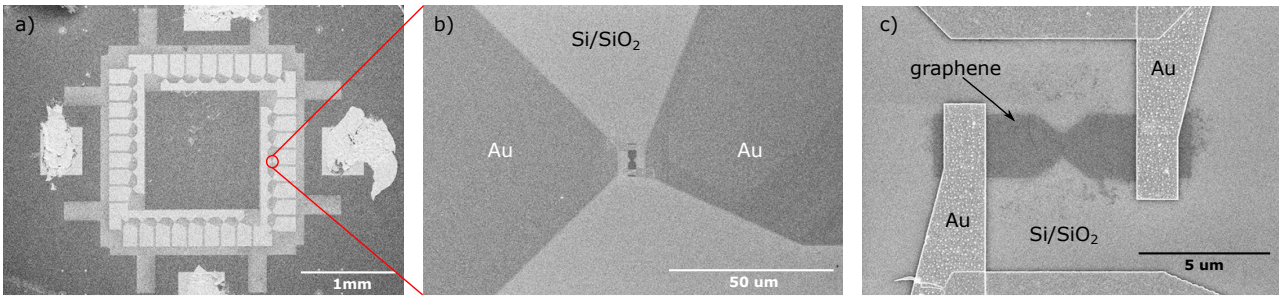


Figure S1: Scanning electron microscopy images of several graphene bridges grouped in a device. The nanogap is open in the bridge by feedback controlled electroburning (see text for details). It typically appears centered around the constriction where heat is dissipated less efficiently.

---

The nanogaps are fabricated on chemical vapor deposited (CVD) graphene films grown on Si/SiO2 substrates. Tens of graphene bridges narrowed at the central part into bow-tie constrictions ($< 1\mu$m) are pre-patterned on the sheets by electron-beam lithography. The surrounding excess graphene is thereafter etched away with oxygen plasma reactive-ion etching. The electrical contact to the resulting graphene bridges is established through gold pads fabricated by electron-beam lithography and subsequent gold deposition. A scanning electron microscope (SEM) image of the resulting devices is shown in Figure S1. The opening of the nanogaps is achieved via a feedback-loop controlled electroburning technique.[1,2] A voltage bias in the few-volts range is applied between the Au terminals at room temperature and in air. The high current density generated heats the flake by Joule effect until eventually some carbon atoms are removed around the constriction where the heat dissipation efficiency is lower.[3,4] As soon as the conductance drops around 10 %, the voltage is ramped to zero in milliseconds to avoid the abrupt burning of the flake that may result in wide gaps. The burning process is repeated until the low bias ($V = 10$ mV) resistance is greater than 10 G$\Omega$ to avoid the presence of graphene nano-islands bridging the electrodes.

Figure S2 shows the $I$ and the derived $\mathrm{d}I/\mathrm{d}V$ color plots measured as a function of the magnetic field and at $T = 2$ K in an additional graphene nano-gap. The appearance of low-bias peaks qualitatively and roughly quantitatively fits with those shown in Figure S2 and the WZ gap scenario described in the main text. Interestingly, a small modulation of the $\mathrm{d}I/\mathrm{d}V$ at varying magnetic field can be observed. This magnetic dependence allows to discard the presence of high spin impurities or quantum-mechanical properties of graphene like the Shubnikov-de Haas effect as explained in the main text.

# 2 Mapping to an extended Hubbard model

We discuss in this section our attempts to explain and fit accurately the DFT electronic structure of our graphene nano-structures by means of extended Hubbard models,

$$\begin{aligned} \hat{H} &= \sum_{i,\delta_n,\sigma} t_n \left( \hat{c}^{\dagger}_{i,\sigma}\, \hat{c}_{i+\delta_n,\sigma} + h.c. \right) + U \sum_{i} \hat{n}_{i,\uparrow}\, \hat{n}_{i,\downarrow} \\ &+ \sum_{i,n} V_n\, \hat{n}_i\, \hat{n}_{i+\delta_n} \end{aligned} \tag{1}$$

where $i$ runs over all lattice sites while $\delta_n$ runs up to $n = 3$ neighbour shells of each site $i$. This is because the conventional Hubbard model could not explain a number of details of our DFT

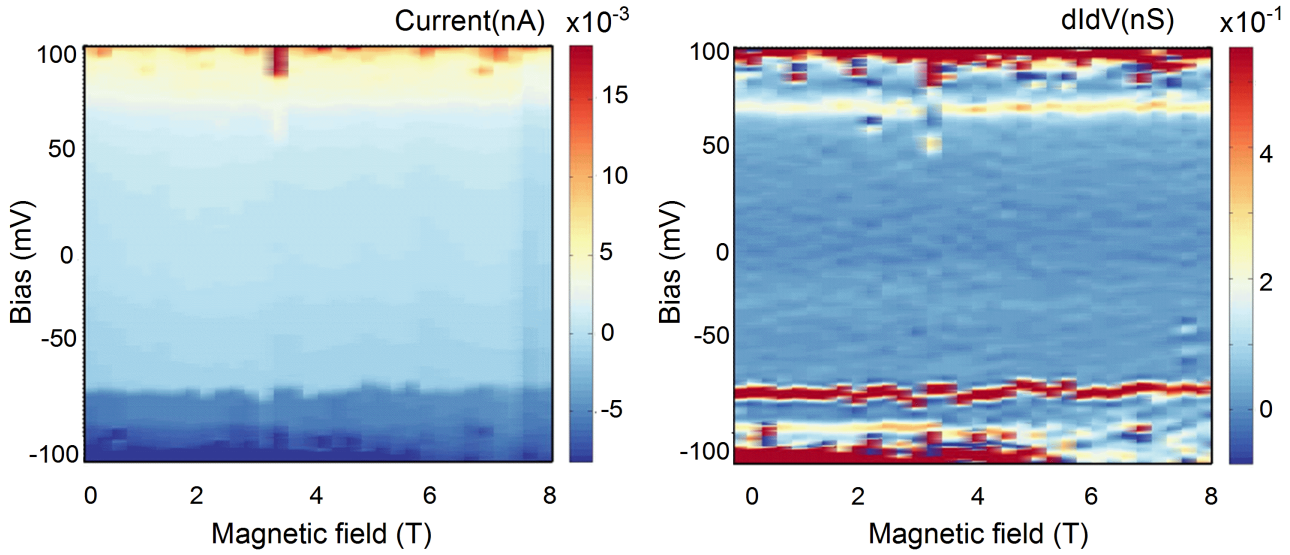


Figure S2: Evolution of the current and the differential conductance of an empty gap as a function of the magnetic field.

---

calculations. Most prominently, our calculations show that electron-hole symmetry is broken in graphene nanogaps, while the half-filled Hubbard model is strictly electron-hole symmetric. Some authors have fitted the LDA electronic structure of graphene ribbons using hoppings and overlaps integrals,[5,6] or have used extended Coulomb integrals $V_n = U/\sqrt{d_{TF}^2 + d_n^2}$ to uncover details of the edge exchange interaction.[7] Here $d_{TF}$ is a Thomas-Fermi screening length and $d_n$ is the distance between atom $i$ and the atoms in the $n$th shell. We have been unable to fit accurately the electronic structure of the islands, ribbons and wedges with the same set of hopping, overlap and Coulomb integrals, even though we went up to the third neighbour shell. We note that adding either hopping $t_2$ or Coulomb $V_2$ integrals breaks the bipartite nature of the lattice so that the system loses electron-hole symmetry.[8,9] We have tested numerically that this is the case by switching on and off $t_2$ and $V_2$.

# 3 Semi-infinite graphene electrodes: conduction channels and edge states

Open Conduction channels (OC) are a cardinal quantity in elastic transport. They provide the number of available electron states of energy $E$ and transverse k-vector $k_t$ coming from the reservoirs and impinging upon the junction. To determine them, we use super-cells containing the elementary unit cell (EUC) as the elementary brick. We show in Figure S3 graphene's reciprocal lattice with the customary hexagonal Brillouin Zone (BZ) and the Dirac points at its corners. The BZ corresponding to the EUC is shown as a black rectangle in the Figure, and the band-structure is determined by folding the hexagon into the rectangle. The six Dirac points reduce to two, that are placed inside the BZ now. Cutting graphene's band structure at a given transverse k-vector delivers one dimensional bands. An example is shown in the top left panel in Figure S4 (a), where the one-dimensional bands at $k_t = 0$ are shown. The corresponding panel on the right plots the number of OC at every energy $E$, that is found by counting the number of bands at that energy. The electrical properties of a junction are determined by summing over all $k_t$. The second row in Figure S4 (a) shows the bands and OC for a calculation that uses the EUC and $n_k = 1440$ $k_t$-points. However, this sort of accurate

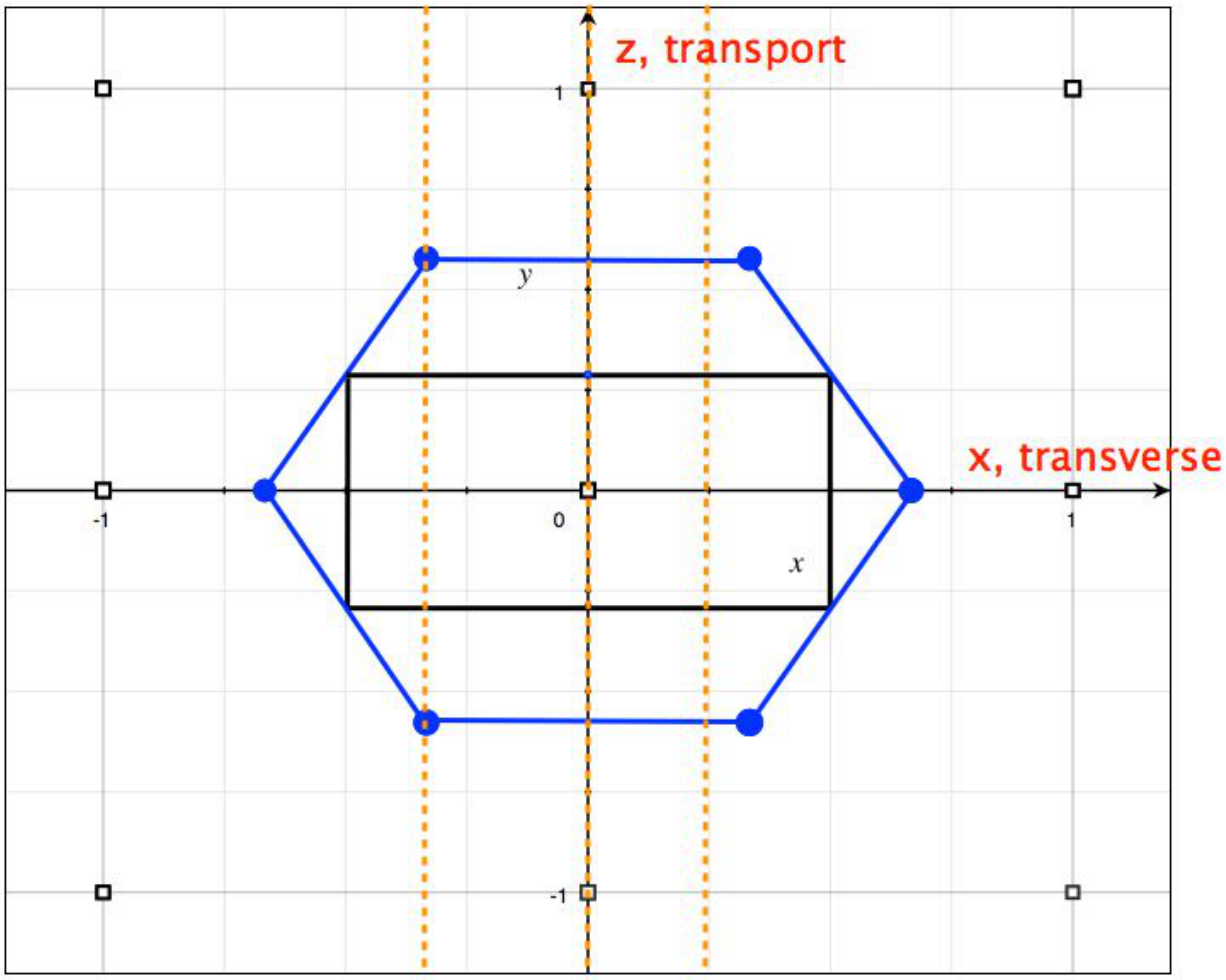


Figure S3: Graphene reciprocal lattice; Blue denotes the conventional unit cell; black denotes the folded unit cell corresponding to EUC; Dotted orange lines denote cuts of the Brillouin zone along specific transverse k-points; the orange line passing through the origin corresponds to a single transverse k-point calculationwith $k_t = 0$; choosing an orange line passing through a Dirac point ensures one channel at zero energy.

---

calculations is infeasible so a smaller number $n_k$ of $k_t$ is chosen, where care must be taken to select one passing through a Dirac point. Alternatively, it is possible to choose a super-cell containing $N_x$ copies of the EUC replicated along the direction transverse to transport. This procedure folds the BZ and band structure $N_x$ times onto itself increasing the number of OC by $N_x$. The third row in Figure S4 (a) shows the bands and OC/$N_x$ in a calculation where a single $k_t = 0$ has been used. The fourth row shows an accurate calculation of OC/$N_x$ with the same $N_x = 9$ super-cell and $n_k = 64$ $k_t$ points.

# 4 Electronic and magnetic properties of a zigzag nanoribbon

The electronic and magnetic properties of hydrogenated zigzag nanoribbons have been discussed extensively in the past. Some of the results of this section are therefore well-established while

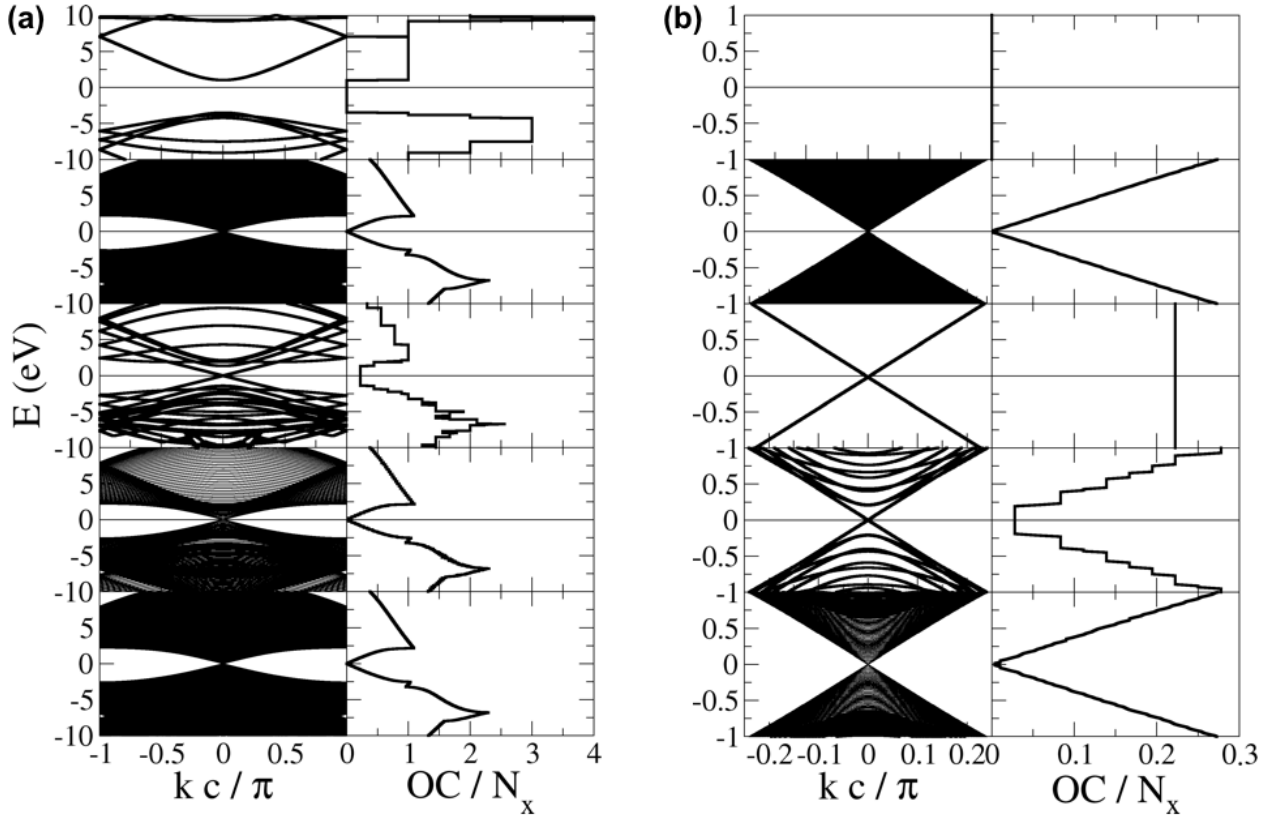


Figure S4: (a) Left and right panel in a given row: one dimensional bands and OC/$N_x$ corresponding to calculations using super-cells with $N_x$ EUCs and $n_k$ transverse $k_t$ points. First row: $N_x = 1$ and $n_k = 1$; second row: $N_x = 1$ and $n_k = 1440$; third row: $N_x = 9$ and $n_k = 1$; fourth row: $N_x = 9$ and $n_k = 64$. (b) Same figure as before, but zoomed over a narrower energy window. The purpose is to show the impact of the different approximations on the distribution of Open Channels along the energy window relevant for the present article,

---

some others are new. Both edges of a zigzag ribbon host spin-polarized edge states, that can have a relative parallel (P) or anti-parallel (AP) spin alignment. Each edge state is associated to a low-energy band whose dispersion is related to the Coulomb interaction.[10,11] The edge bands are spin polarized, display a mean field gap and extend within the energy window $[-0.4, 0.15]$ eV as shown in Figure 4 in the main text. This means that they could contribute a priori to deliver a spin signature in the low-voltage electrical transport of our ZZ nanogaps.

Our DFT VASP (SIESTA) results shed a magnetic moment for each of the two carbon atoms at the edge of $m_A = 0.26$ (0.25) $\mu_B$ and $m_B = -0.04$ (-0.03) $\mu_B$. The total moment per unit cell is $0.56\,\mu_B$, that takes into account the decay of magnetization towards the center of the ribbon. These magnetic moments are slightly smaller than, but consistent with, previous estimates.[10,12] VASP yields a magnetic anisotropy energy per unit cell $D$ below 0.01 $\mu$eV. SIESTA also sheds $D \leq 1\,\mu$eV. Our values for $D$ are at least two orders of magnitude smaller than previous estimates,[13] and impact predictions on the edge transport properties.[14] Our results are also consistent with the fact that the anisotropy Hamiltonian of spin 1/2 localized electrons delivers trivially a zero energy barrier: $\hat{H} = D\,\hat{S}_Z^2 = D\,\hat{I}$, where $\hat{I}$ is the two-dimensional identity matrix.

We expect that the experimentally realized edges have defects that will split them into independent segments of average length $L$ unit cells. In consequence, we find that the magnetic properties of hydrogen passivated edge states is governed by an ensemble of purely isotropic

Heisenberg chains of length $L$. These should obey super-paramagnetic behaviour with a tiny switching time of the order of nanoseconds at any temperature above 1 K. Magnetization reversal events can be driven by coherent rotation processes if $L \leq L_c$ or by soliton-antisoliton nucleation if $L \geq L_c$.[15–17] To estimate the critical length $L_c \sim 4\sqrt{J/D}$ we pick $J = 100$ meV as estimated by Yazyev and Kastnelson.[12] Because we expect $D$ to be below $10^{-8}$ eV, we find a critical length $L_c$ exceeding hundreds of nanometers, and certainly larger than any imaginable $L$. In consequence, we expect that the edge-state spin dynamics will be driven by coherent rotation processes.

# 5 Magnetic properties of a ZZ nanogap

We have estimated the exchange interaction $J_{\rm gap}$ across ZZ nanogaps as a function of the gap length $d = d_0$. Here we have set the atomic spins at the edges parallel and anti-parallel to each other (P ar AP, respectively) and computed their energy difference. We have found that $J_{\rm gap}$ follows an exponential behaviour with $d$ that favours an AP alignment as expected,

$$J_{\rm gap} = J_0\, e^{-d/l_{\rm exch}} = 22\, e^{-d({\rm \AA})/3{,}8}\, \mu{\rm eV} \tag{2}$$

Hence the energy barrier for magnetization reversal is truly small. To achieve an intuition of the order of magnitude of the room temperature switching time $\tau$ we use an Arrhenius law

$$\tau = \tau_0\, e^{L\, J_{\rm gap}/K_{\rm B}\, T} = \tau_0\, e^{L\, e^{-d/3.8}/4\, T} \tag{3}$$

where $\tau_0$ is an intrinsic time that we guess to be of order of nanoseconds, and $L$ and $d$ are measured in unit cells and Å, respectively. We find that $\tau \sim \tau_0$ even for almost defect-free edges ($L \sim 1000$) and gaps lengths $d$ as short as 1.5 nm. Conversely, we wish to estimate the blocking Temperature $T_{\rm B}$ below which we could find AP ordering experimentally

$$T_{\rm B,gap} \sim \frac{L\, e^{-d/3.8}}{4\, \ln(\tau/\tau_{0,{\rm gap}})}\, {\rm K} \tag{4}$$

We pick a gap length of $d \sim 1.5$ nm and set $\tau$ to be of the order of hours and find that $T_{\rm B} \sim 10^{-4}\, L$ K, e.g.: a blocking temperature below 1 K even for quite defect-less edges.

Summarizing, we expect that the spin alignment at the junction will be fluctuating between P and AP configurations at any laboratory temperature. This sort of super-paramagnetic behaviour could be lifted in favour of a P alignment either by a large magnetic field of order $H \sim K_{\rm B}\, T/\mu_{\rm B}$ or by a large current flowing through the junction via the spin-toque effect.

# 6 A one-dimensional model

The essential features of the electrical response of graphene nanogaps can be encapsulated via a one-dimensional model,[18] that we show schematically in Figure S5. The graphene reservoirs are described by a semi-infinite chain having a single spin-unpolarized atomic level per site placed at zero energy to reflect electron-hole symmetry. The reservoirs are connected to a single level placed at the graphene edge. The state shows a slight electron-hole asymmetry and spin-polarization as discussed in the main text. The strong coupling of this state to the other levels in the chain, the asymmetry and the polarization give spin-up and down transmissions in the ZZ configuration that are rather flat and cross each other below the Fermi level. A wedge is represented by another level placed at the edge having a much larger spin polarization and electron-hole asymmetry. This state is, however, weakly coupled to the other states in the chain. Such weak coupling gives rise to transport resonances that are clearly seen as two peaks

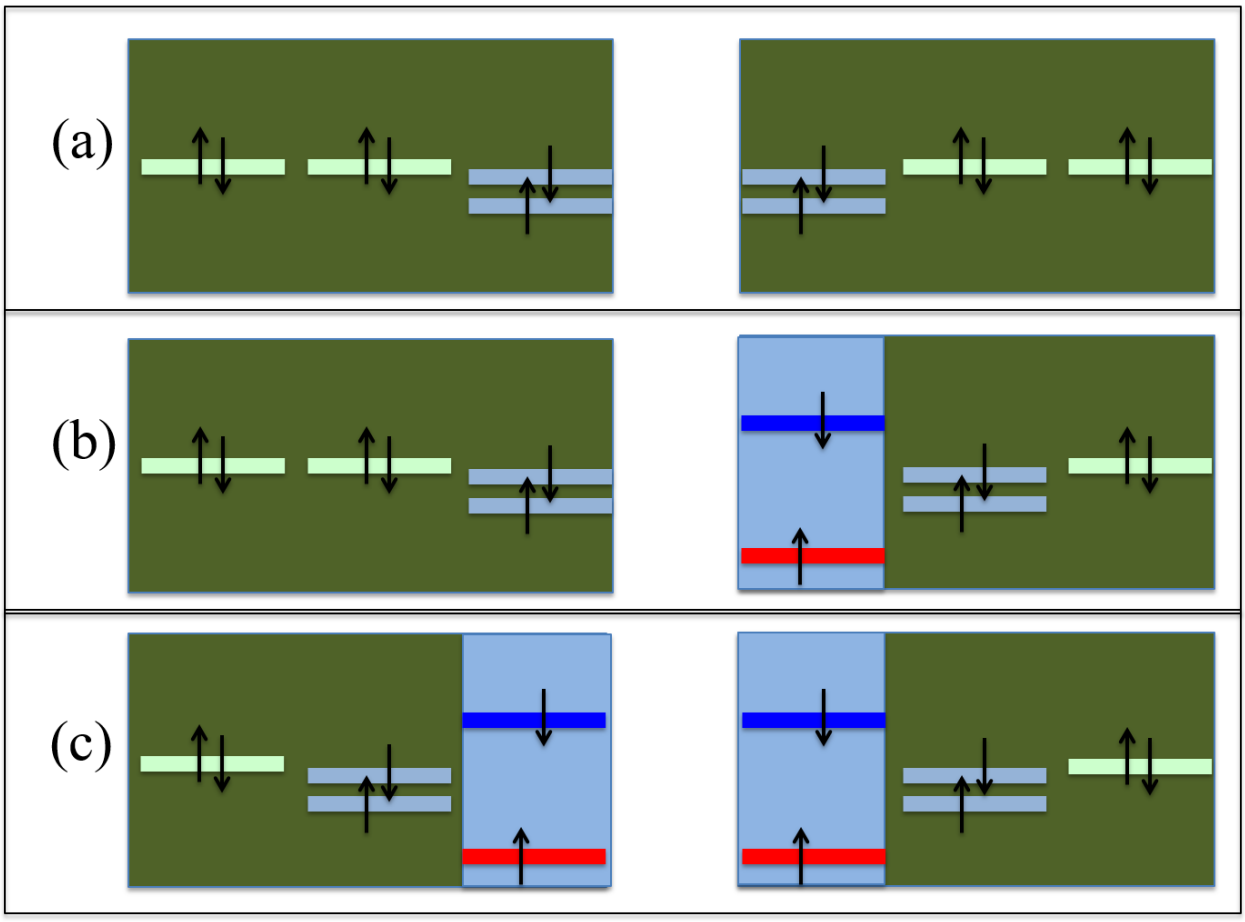


Figure S5: Schematic representation of the energy spectrum of the one-dimensional model used to describe the transport properties of the different nanogaps: (a) ZZ nanogaps. Here, conduction channels at the electrodes have electron-hole symmetry and are spin-unpolarized, while states closer to the gaps lose both electron-hole and spin-symmetry. (b) WZ nanogaps display in addition a M1 wedge state localized at the left electrode. (c) WW nanogaps show M1 wedge states at both electrodes.

---

in the WZ and WW configurations, one for each spin. Transport calculations with this model show that it can reproduce accurately the electrical response of ZZ, WZ and WW nanogaps derived from the DFT simulations (for a single $n_k = 1$ transverse k-point calculation), if we fine-tune the model parameters.

A model of this sort reproduces nicely the Transmission curves shown in Figures 7 and 9 in the main text. Specifically, the model comprises the two one-dimensional electrodes, two one-dimensional segments of 28 atoms each at the scattering region. These segments are terminated by the localized levels described above at each side of the gap. We have ramped up the gate voltage at this central part of the scattering region. We have introduced a mismatch between the on-site energies of the electrodes and the scattering region atoms of 1.0 eV because we wanted to account for Fabry-Pérot resonances. We find that these interferences in our model are prominent only for ZZ nanogaps. Those fringes are masked in WZ and WW nanogaps by the conductance peaks originated by the M1 localized mode.

# References


[1] F. Prins, A. Barreiro, J. W. Ruitenberg, J. S. Seldenthuis, N. Aliaga-Alcalde, L. M. K. Vandersypen and H. S. J. van der Zant, *Nano Lett.*, 2011, **11**, 4607–4611.

[2] E. Burzurí, F. Prins and H. S. J. van der Zant, *Graphene*, 2012, **01**, 26–29.

[3] J. O. Island, A. Holovchenko, M. Koole, P. F. A. Alkemade, M. Menelaou, N. Aliaga-Alcalde, E. Burzurí and H. S. J. van der Zant, *J. Phys. Condens. Matter*, 2014, **26**, 474205.

[4] E. Burzurí, J. O. Island, R. Díaz-Torres, A. Fursina, A. González-Campo, O. Roubeau, S. J. Teat, N. Aliaga-Alcalde, E. Ruiz and H. S. J. van der Zant, *ACS Nano*, 2016, **10**, 2521–2527.

[5] S. Reich, J. Maultzsch, C. Thomsen and P. Ordejón, *Phys. Rev. B*, 2002, **66**, 035412.

[6] Y. Hancock, A. Uppstu, K. Saloriutta, A. Harju and M. J. Puska, *Phys. Rev. B*, 2010, **81**, 245402.

[7] J. Jung, *Phys. Rev. B*, 2011, **83**, 165415.

[8] A. Mielke, *Modeling and Simulation*, 2015, **5**, 1.

[9] J. K. Asboth, L. Oroszlany and A. Palyi, *A short course on Topological Insulators: band-structure topology and edge states in one and two dimensions*, Lecture Notes in Physics, 919, 2016.

[10] L. Pisani, J. A. Chan, B. Montanari and N. M. Harrison, *Phys. Rev. B*, 2007, **75**, 064418.

[11] J. Fernandez-Rossier, *Physical Review B*, 2008, **77**, 075430.

[12] O. V. Yazyev and L. Helm, *Phys. Rev. B*, 2007, **75**, 125408.

[13] O. V. Yazyev and M. I. Kastnelson, *Phys. Rev. Lett.*, 2008, **100**, 047209.

[14] J. L. Lado and J. Fernández-Rossier, *Phys. Rev. Lett.*, 2014, **113**, 027203.

[15] H. B. Braun, *Phys. Rev. B*, 1994, **50**, 16485.

[16] H. B. Braun, *Phys. Rev. B*, 1994, **50**, 16501.

[17] D. Hinzke and U. Nowak, *Phys. Rev. B*, 2000, **61**, 6734.

[18] S. Martín, D. Z. Manrique, V. M. García-Suárez, W. Haiss, S. J. Higgins, C. J. Lambert and R. J. Nichols, *Nanotechnology*, 2009, **20**, 125203.